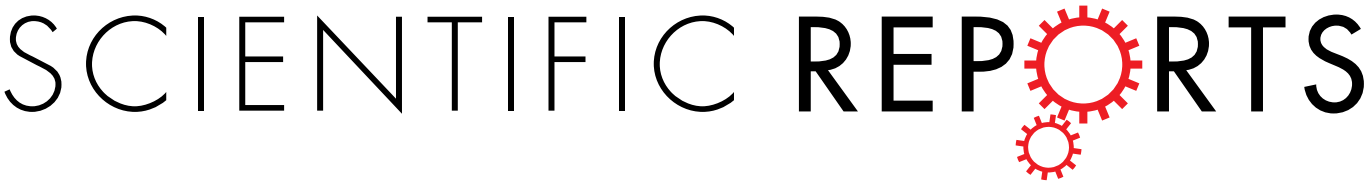

OPEN

Two-band and pauli-limiting effects on the upper critical field of 112-type iron pnictide superconductors

Received: 19 January 2017
Accepted: 07 March 2017
Published: 06 April 2017

Xiangzhuo Xing[1], Wei Zhou[1], Jinhua Wang[2], Zengwei Zhu[2], Yufeng Zhang[1], Nan Zhou[1], Bin Qian[3], Xiaofeng Xu[3] & Zhixiang Shi[1]

The temperature dependence of upper critical field μ_0H_{c2} of $Ca_{0.83}La_{0.17}FeAs_2$ and $Ca_{0.8}La_{0.2}Fe_{0.98}Co_{0.02}As_2$ single crystals are investigated by measuring the resistivity for the inter-plane (*H//c*) and in-plane (*H//ab*) directions in magnetic fields up to 60T. It is found that $\mu_0H_{c2}(T)$ of both crystals for *H//c* presents a sublinear temperature dependence with decreasing temperature, whereas the curve of $\mu_0H_{c2}(T)$ for *H//ab* has a convex curvature and gradually tends to saturate at low temperatures. $\mu_0H_{c2}(T)$ in both crystals deviates from the conventional Werthamer-Helfand-Hohenberg (WHH) theoretical model without considering spin paramagnetic effect for *H//c* and *H//ab* directions. Detailed analyses show that the behavior of $\mu_0H_{c2}(T)$ in 112-type Iron-based superconductors (IBSs) is similar to that of most IBSs. Two-band model is required to fully reproduce the behavior of $\mu_0H_{c2}(T)$ for *H//c*, while the effect of spin paramagnetic effect is responsible for the behavior of $\mu_0H_{c2}(T)$ for *H//ab*.

Recently, the newly discovered 112-type Iron-based superconductors (IBSs) $Ca_{1-x}RE_xFeAs_2$ (RE = rare-earth elements) have attracted tremendous interest due to their peculiar properties compared with other IBSs[1,2]. It crystallizes in a monoclinic crystal structure with a space group of P_{21}, consisting of alternating stacking of FeAs and As zigzag bond layers. The FeAs layers have been proven to be responsible for the High-T_c superconductivity, while the unique As zigzag bond layers could generate anisotropic Dirac cones, and an additional three-dimensional (3 D) hole pocket which is absent in other IBSs[3–5], and may also be possible for realizing the Majorana related physics[6]. However, so far the pair mechanism and many basic physical properties both in the superconducting and normal states are still not well understood in this compound. Upper critical field μ_0H_{c2}, is one of the most important superconducting parameters for gathering an understanding of unconventional superconductivity including coherence length, coupling strength, and insights into the pair-breaking mechanism. Moreover, the anisotropy of μ_0H_{c2}, which is related to the dimensionality and the topology of the underlying electronic structure, also becomes important for potential applications as well as for understanding multiband effects. Many efforts have been made to investigate the $\mu_0H_{c2}(T)$ ever since the discovery of IBSs[7]. For instance, in 1111-type IBSs, $\mu_0H_{c2,c}(T)$ shows a significant upturn behavior in (La, Nd)FeAs(O,F)[8,9], and linearly increases with decreasing temperature but tends to be saturated at low temperatures in SmFeAs(O,F)[10]. Both behaviors can be accounted by the two-band theory[11]. $\mu_0H_{c2,ab}(T)$ exhibits a downturn and flattening curvature with decreasing temperature, which is mainly ascribed to the spin-paramagnetic effect[10,12]. For 122-type and 111-type IBSs, $\mu_0H_{c2,c}(T)$ exhibits a linear increase down to the lowest temperature, and $\mu_0H_{c2,ab}(T)$ also shows a downturn curvature with decreasing temperature. These behaviors can also be interpreted using the two-band theory and spin-paramagnetic effect, respectively[13–17]. Furthermore, spin-paramagnetic effect dominates in both of $\mu_0H_{c2,ab}(T)$ and $\mu_0H_{c2,c}(T)$ in the 11-type IBSs(e.g., $Fe_{1+y}Te_{1-x}Se_x$)[18,19]. Nevertheless, the behavior of $\mu_0H_{c2}(T)$ at high fields and low temperatures is not clear yet in this newly discovered 112-type IBSs. Therefore, it is interesting to check whether $Ca_{1-x}RE_xFeAs_2$ may represent a new type of IBSs, because the multiband electronic structure and peculiar properties in $Ca_{1-x}RE_xFeAs_2$ may contribute to the behavior of upper critical filed.

Previous studies of $\mu_0H_{c2}(T)$ were just performed near T_c in low magnetic field[20,21]. Thus, measurement in higher magnetic field is essential to clarify the behavior of upper critical field and its anisotropy γ at low

[1]Department of Physics and Key Laboratory of MEMS of the Ministry of Education, Southeast University, Nanjing 211189, China. [2]Wuhan National High Magnetic Field Center, School of Physics, Huazhong University of Science and Technology, Wuhan 430074, China. [3]Advanced Functional Materials Lab and Department of Physics, Changshu Institute of Technology, Changshu 215500, China. Correspondence and requests for materials should be addressed to B.Q. (email: njqb@cslg.edu.cn) or Z.S. (email: zxshi@seu.edu.cn)

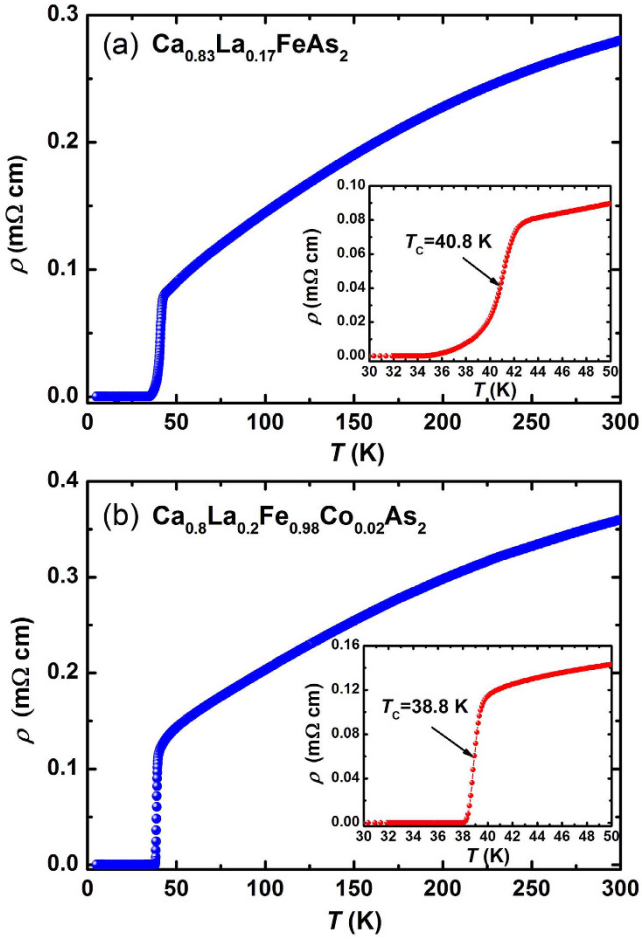

Figure 1. Temperature dependence of the in-plane electrical resistivity $\rho(T)$ for (**a**) $Ca_{0.83}La_{0.17}FeAs_2$ and (**b**) $Ca_{0.8}La_{0.2}Fe_{0.98}Co_{0.02}As_2$ single crystals at zero field. The insets of (**a**) and (**b**) show an enlarged view of resistivity near the superconducting transition, T_c was determind by the 50% normal state resistivity ρ_n.

temperature region in this new type IBSs. Benefiting from the advanced technology of pulsed field measurement, in this work, we reported the temperature dependence of upper critical field $\mu_0 H_{c2}(T)$ of $Ca_{0.83}La_{0.17}FeAs_2$ and $Ca_{0.8}La_{0.2}Fe_{0.98}Co_{0.02}As_2$ single crystals by measuring the electrical resistivity in pulsed fields up to 60 T at Wuhan National High Magnetic Field Center. The behavior of $\mu_0 H_{c2}(T)$ and its anisotropy are systematically studied. Our results suggest that the two-band and spin-paramagnetic effects are shown to be responsible for the temperature-dependent behavior of $\mu_0 H_{c2,c}(T)$ and $\mu_0 H_{c2,ab}(T)$, respectively.

Results

Figure 1 presents the temperature dependence of the in-plane resistivity $\rho(T)$ at zero field for (a) $Ca_{0.83}La_{0.17}FeAs_2$ and (b) $Ca_{0.8}La_{0.2}Fe_{0.98}Co_{0.02}As_2$ single crystals. The resistivity of both crystals monotonically decreases with decreasing temperature and shows no anomaly corresponding to the antiferromagnetic (AFM)/structural transition down to T_c. The insets show the enlarged view near the superconducting transition. The transition temperature is estimated as $T_c^{50\%} = 40.8$ K for $Ca_{0.83}La_{0.17}FeAs_2$ and $T_c^{50\%} = 38.8$ K for $Ca_{0.8}La_{0.2}Fe_{0.98}Co_{0.02}As_2$. The transition width ΔT_c, determined by adopting the criterion of $90\%\rho_n$–$10\%\rho_n$, is 3.8 K for $Ca_{0.83}La_{0.17}FeAs_2$, larger than the value of 1.1 K for $Ca_{0.8}La_{0.2}Fe_{0.98}Co_{0.02}As_2$. The slightly wide superconducting transition for $Ca_{0.83}La_{0.17}FeAs_2$ seems to be a general feature in this compound, which may result from the inhomogeneity of La distribution. Upon a small amount of Co doping, single crystal quality can be improved significantly with sharp superconducting transition and large superconducting volume fraction[20–23].

Figure 2 shows the temperature dependence of the in-plane resistivity $\rho(T)$ of $Ca_{0.83}La_{0.17}FeAs_2$ and $Ca_{0.8}La_{0.2}Fe_{0.98}Co_{0.02}As_2$ single crystals in low magnetic fields from 0 to 9 T for $H//ab$ and $H//c$. With increasing fields, the resistivity transition width becomes broader and the onset of superconductivity shifts to lower temperatures gradually. It is worth noting that the superconducting transitions of $Ca_{0.83}La_{0.17}FeAs_2$ and $Ca_{0.8}La_{0.2}Fe_{0.98}Co_{0.02}As_2$ show different response to the increased magnetic field. For $Ca_{0.8}La_{0.2}Fe_{0.98}Co_{0.02}As_2$, the field-induced broadening of superconducting transition is more pronounced for $H//c$, showing a tail structure at low temperatures, similar to the case in 1111-type IBSs and cuprates, which can be explained in terms of the formation of vortex-liquid phase[8,10,24,25]. In contrast, for $Ca_{0.83}La_{0.17}FeAs_2$, the transition shows slightly field-induced broadening, indicating the vortex-liquid state region is very narrow, similar to the results of 122-type and 11-type

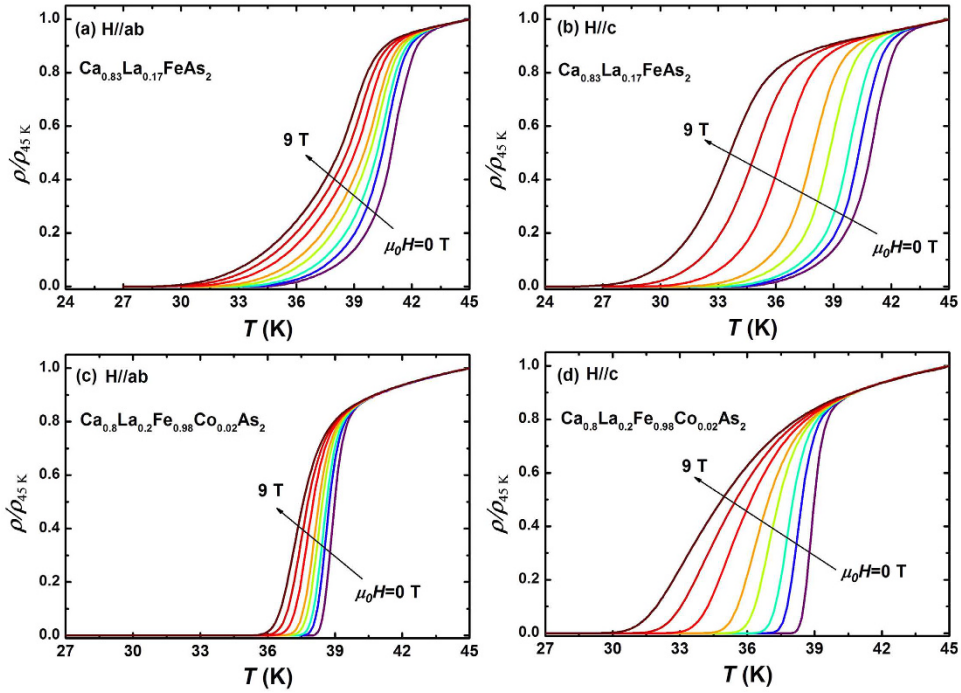

Figure 2. Temperature dependence of in-plane resistivity (nomalized to 45 K) of $Ca_{0.83}La_{0.17}FeAs_2$ for (**a**) *H*//*ab* and (**b**) *H*//*c*, and of $Ca_{0.8}La_{0.2}Fe_{0.98}Co_{0.02}As_2$ for (**c**) *H*//*ab* and (**d**) *H*//*c* at the various magnetic fields from 0 to 9 T(0, 0.5, 1, 2, 3, 5, 7 and 9 T).

IBSs[18,26–29]. This discrepancy seems to be consistent with the different vortex dynamics in both samples. Indeed, a small amount of Co doping distinctly influences the vortex dynamics and flux pinning, in comparison with $Ca_{0.83}La_{0.17}FeAs_2$, the second magnetization peak was clearly observed and critical current density enhanced significantly through introducing more effective pinning center in $Ca_{0.8}La_{0.2}Fe_{0.98}Co_{0.02}As_2$[23,30].

The magnetic field dependence of resistivity $\rho(H)$ of $Ca_{0.83}La_{0.17}FeAs_2$ and $Ca_{0.8}La_{0.2}Fe_{0.98}Co_{0.02}As_2$ single crystals for *H*//ab and *H*//c are presented in Fig. 3. Since there is no hysteresis for $\rho(H)$ under μ_0H sweep up and down processes, only data collected during the down sweep of the magnet are shown. Obviously, the superconducting transitions are suppressed upon increasing magnetic field for both directions. In addition, the superconductivity of $Ca_{0.8}La_{0.2}Fe_{0.98}Co_{0.02}$ is more robust against magnetic field compared with $Ca_{0.83}La_{0.17}FeAs_2$, indicating $Ca_{0.8}La_{0.2}Fe_{0.98}Co_{0.02}As_2$ has a higher $\mu_0H_{c2}(0)$ than $Ca_{0.83}La_{0.17}FeAs_2$.

In order to minimize the effects of superconducting fluctuation near 90%ρ_n and vortex motion in the vortex-liquid region near 10%ρ_n on the determination of μ_0H_{c2}, we use the 50%ρ_n criteria, which is widely accepted to be close to the real μ_0H_{c2}, to define the $\mu_0H_{c2}(T)$ values in the following[10,31]. The normal state resistivity ρ_n was determined by linearly extrapolating the normal state resistivity into the superconducting state in $\rho(T)$ and $\rho(H)$ curves separately. $\mu_0H_{c2}(T)$ of both crystals for *H*//*ab* and *H*//*c* directions along with the low magnetic field data up to 9 T were shown in Fig. 4. $\mu_0H_{c2}(T)$ obtained from the pulsed field measurement follows well the curvature and values of the low filed ones. Data above 60 T were extracted by linear extrapolation of $\rho(H)$ at $\mu_0H < 60$ T to $\rho(H) = 0.5\rho_n(T_c, H)$[18,32]. In several highly two-dimensional superconductors, the curvature of $\mu_0H_{c2}(T)$ has been reported to vary depending on the criteria used to determine μ_0H_{c2}[8,14]. Thus, the $\mu_0H_{c2}(T)$ defined by 80%ρ_n and 20%ρ_n were also presented in Supplementary Information (SI), Fig. S2. It is noted that the shape of $\mu_0H_{c2}(T)$ curve does not change qualitatively when $\mu_0H_{c2}(T)$ is defined by different criteria in this compound. In addition, a slight upward behavior near T_c which commonly observed in some IBSs[14,33,34], is also observed for both directions, might be due to the flux dynamics as is seen in cuprates[35].

Discussion

Generally, two distinct mechanisms exist in superconductivity suppression under magnetic fields in type-II superconductors. One is the orbital pair-breaking effect, with opposite momenta acting on the paired electrons. In this case, the superconductivity is destroyed when the kinetic energy of the Cooper pairs exceeds the condensation energy. The other is attributed to the spin-paramagnetic pair-breaking effect, which comes from the Zeeman splitting of spin singlet cooper pairs. The superconductivity is also eliminated when the Pauli spin susceptibility energy is larger than the condensation energy. WHH theory, which could identify the contribution of each pair-breaking mechanism, was used to fit the $\mu_0H_{c2}(T)$ curves, and the strength of the spin-paramagnetic effect and the spin-orbit effect were incorporated via the Maki parameter α and the spin-orbit interaction λ_{so}, respectively[36]. According to the WHH theory, $\mu_0H_{c2}(T)$ in the dirty limit can be described by the digamma function[37]

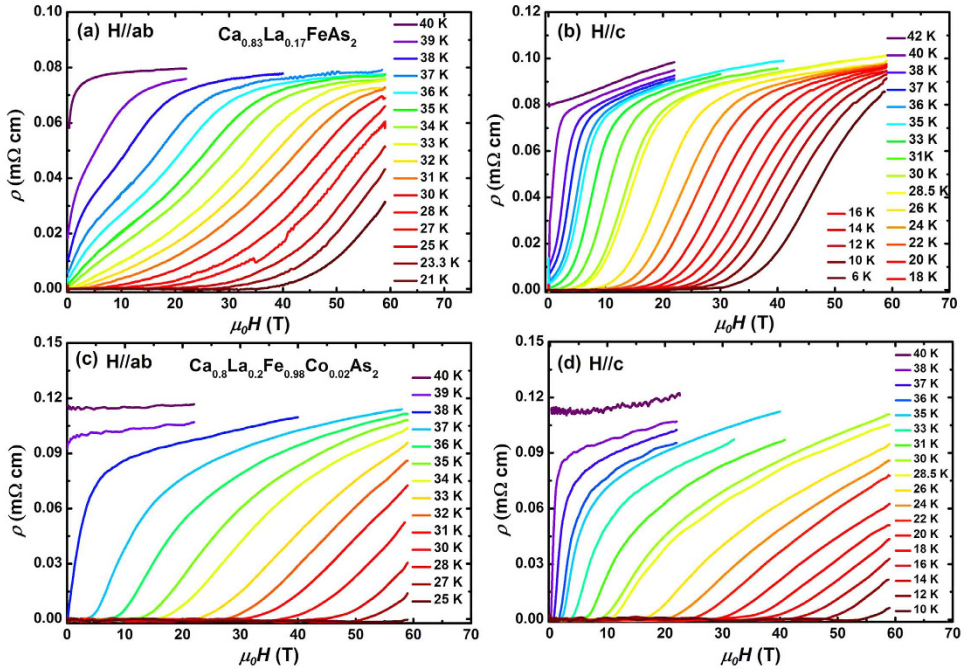

Figure 3. Magnetic field dependence of in-plane resistivity $\rho(H)$ of $Ca_{0.83}La_{0.17}FeAs_2$ for (**a**) H//ab and (**b**) H//c, and of $Ca_{0.8}La_{0.2}Fe_{0.98}Co_{0.02}As_2$ for (**c**) H//ab and (**d**) H//c measured at fixed temperatures in pulsed fields up to 60 T.

$$\ln\frac{1}{t}=\left(\frac{1}{2}+\frac{i\lambda_{so}}{4\gamma}\right)\Psi\left(\frac{1}{2}+\frac{\bar{h}+\lambda_{so}/2+i\lambda}{2t}\right)+\left(\frac{1}{2}-\frac{i\lambda_{so}}{4\gamma}\right)\Psi\left(\frac{1}{2}+\frac{\bar{h}+\lambda_{so}/2-i\lambda}{2t}\right)-\Psi\left(\frac{1}{2}\right) \quad (1)$$

where $t=T/T_c$, $\gamma\equiv[(\alpha\bar{h})^2-(\lambda_{so}/2)^2]^{1/2}$ and $\bar{h}=\frac{4\bar{h}}{\pi^2(-d\bar{h}/dt)_{t=1}}=\frac{4H_{c2}}{\pi^2(-dH_{c2}/dt)_{t=1}}$.

In the absence of both spin-paramagnetic effect and spin-orbit interaction, $\alpha=0$ and $\lambda_{so}=0$, the orbital-limited upper critical field is expressed as

$$\mu_0H_{c2}^{orb}=-0.693\left(\frac{dH_{c2}}{dT}\right)_{T=T_c} \quad (2)$$

In the weakly coupled BCS superconductors, the pauli limited field is given by[38]

$$\mu_0H_p(0)=\mu_0H_p^{BCS}(0)=1.84\ T_c\ [\mathrm{K}] \quad (3)$$

For conventional superconductors, μ_0Hp (0) is usually much larger than $\mu_0H_{c2}^{orb}$ (0), and therefore, their upper critical field is mainly restricted by the orbital pair breaking mechanism. While, the spin-paramagnetic effect may play an import role in pair breaking in some unconventional superconductors[10,12,14–19]. In our case, we obtained $\mu_0H_p^{BCS}(0)=75$ T for $Ca_{0.83}La_{0.17}FeAs_2$ and $\mu_0H_p^{BCS}(0)=71.4$ T for $Ca_{0.8}La_{0.2}Fe_{0.98}Co_{0.02}As_2$. The slope values of $d\mu_0H_{c2}/dT$ near T_c is 3.98 T/K (9.22 T/K) and 1.23 T/K (2.26 T/K) for H//ab and H//c in $Ca_{0.83}La_{0.17}FeAs_2$ ($Ca_{0.8}La_{0.2}Fe_{0.98}Co_{0.02}As_2$), respectively. Using the WHH model, i.e. Eq. (2), one can estimate the orbital limited upper critical fields, which gives $\mu_0H_{c2,ab}^{orb}(0)=112.5$ T (248 T) and $\mu_0H_{c2,c}^{orb}(0)=34.9$ T (60.9 T) for $Ca_{0.83}La_{0.17}FeAs_2$ ($Ca_{0.8}La_{0.2}Fe_{0.98}Co_{0.02}As_2$). In both crystals, the values of $\mu_0H_{c2,c}^{orb}(0)$ are much smaller than the corresponding $\mu_0H^{BCS}{}_p(0)$. In contrast, $\mu_0H_{c2,ab}^{orb}(0)$ is much larger than $\mu_0H_p^{BCS}(0)$. Thus, it is likely that the upper critical field in both crystals is limited by the orbital effect for H//c, but is limited by the spin paramagnetic for H//ab.

As evidenced from Fig. 4, the experimental $\mu_0H_{c2}(T)$ curves of both crystals deviate from the WHH model neglecting the spin paramagnetic effect ($\alpha=0$) and spin-orbit interaction ($\lambda_{so}=0$) in H//ab and H//c at low temperatures (dotted lines). For H//ab, the curve of $\mu_0H_{c2}(T)$ falls below the WHH model ($\alpha=0$ and $\lambda_{so}=0$) and has a tendency to saturate at low temperatures, indicating the spin-paramagnetic effect should be considered, as we discussed above. The best fits (dashed lines) were obtained using Eq. (1) with $\alpha=0.9$ for $Ca_{0.83}La_{0.17}FeAs_2$, and $\alpha=1.9$ for $Ca_{0.8}La_{0.2}Fe_{0.98}Co_{0.02}As_2$. It is noteworthy here that the spin-orbit scattering is not necessary to have the best fit ($\lambda_{so}=0$). The negligible value of λ_{so} compared to the other IBSs indicates the spin-orbit scattering is also rather weak in this compound[10,12,16,18,32]. According to Maki[36], the paramagnetic limited field $\mu_0H_{c2}^P(0)$ expresses as $\mu_0H_{c2}^P(0)=\mu_0H_{c2}^{orb}(0)/\sqrt{1+\alpha^2}$, where the Maki parameter α, is given by $\alpha=\sqrt{2}H_{c2}^{orb}(0)/H_p(0)$, $\mu_0H_p(0)$ is the zero temperature pauli limited field. The values of $\mu_0H_{p,ab}(0)$ using α obtained from WHH model fitting for

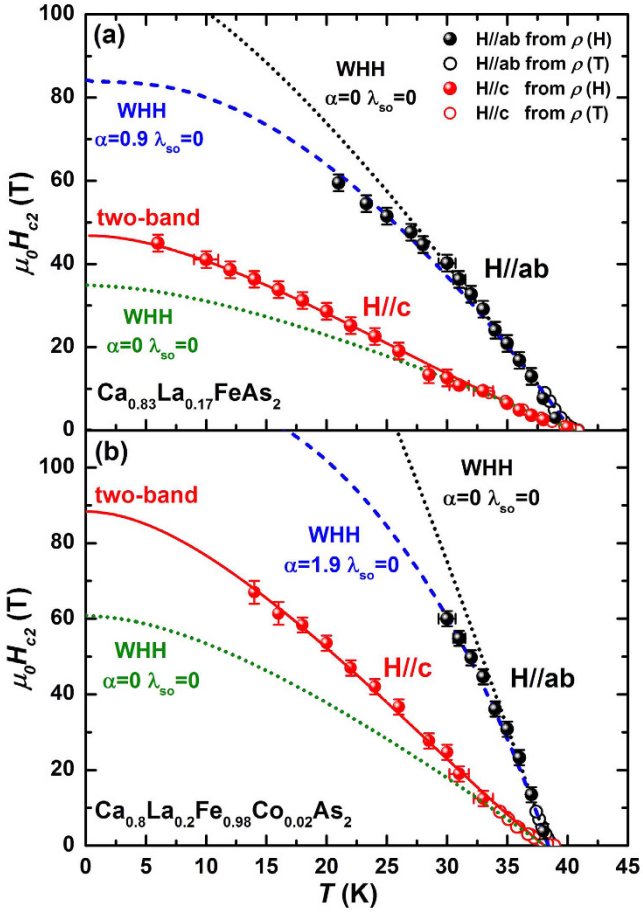

Figure 4. The upper critical field $\mu_0 H_{c2}(T)$ versus temperature for (**a**) $Ca_{0.83}La_{0.17}FeAs_2$ and (**b**) $Ca_{0.8}La_{0.2}Fe_{0.98}Co_{0.02}As_2$ single crystals. Symbols of the open circles and filled circles represent the data obtained in the low magnetic field and pulsed field, respectively. The dotted lines are the WHH fits neglecting the spin paramagnetic effect for *H*//*ab* and *H*//*c*, respectively, while the dashed lines are the best fits to the experimental data by WHH model with the pauli-limiting effect considered for *H*//*ab*. The solid lines for *H*//*c* are fitting to the data using the two-band model.

$Ca_{0.83}La_{0.17}FeAs_2$ and $Ca_{0.8}La_{0.2}Fe_{0.98}Co_{0.02}As_2$ are 176.75 T and 184.56 T, respectively, larger than the corresponding $\mu_0 H_p^{BCS}(0)$ in both crystals. In IBSs, the weak-coupling BCS formula usually underestimates the actual paramagnetic limit. This enhancement of pauli limited field seems to be a common feature in IBSs, presumably aroused by many-body correlation and the strong coupling effects in IBSs[12,16,18].

For *H*//*c*, $\mu_0 H_{c2,c}(T)$ shows an almost linear temperature dependence and tends to be saturated at low temperatures, similar to the results of 1111-type SmFeAs(O,F) single crystals[10]. At low temperatures, the $\mu_0 H_{c2,c}(T)$ is slightly larger than the value predicted with Eq. (2). The sublinear increase and enhancement of $\mu_0 H_{c2,c}(T)$ are generally observed in many multiband superconductors, e.g., MgB_2 and some IBSs[8–10,14,17,39,40], which has been successfully explained by the two-band model[11]. The equation of $\mu_0 H_{c2}(T)$ for a two-band superconductor is given by:

$$a_0[lnt + U(h)][lnt + U(\eta h)] + a_1[lnt + U(h)] + a_2[lnt + U(\eta h)] = 0, \quad (4)$$

where $t = T/T_c$, $a_0 = 2(\lambda_{11}\lambda_{22} - \lambda_{12}\lambda_{21})/\lambda_0$, $a_1 = 1 + (\lambda_{11} - \lambda_{22})/\lambda_0$, $a_2 = 1 - (\lambda_{11} - \lambda_{22})/1/2\,\lambda_0$, $\lambda_0 = ((\lambda_{11} - \lambda_{22})^2 + 4\lambda_{12}\lambda_{21})^{1/2}$, $h = H_{c2}D_1/(2\Phi_0/T)$, $\eta = D_2/D_1$ and $U(x) = \Psi(1/2 + x) - \Psi(1/2)$. $\Psi(x)$ is the digamma function, D_1 and D_2 are the diffusivity of each band, λ_{11}, λ_{22} denote the intra-band coupling constants, and λ_{12}, λ_{21} are the inter-band coupling constants. Due to the lack of microscopic theory of pairing mechanism, we choose the values of λ referring to previous reports in SmFeAs(O,F) from ref. 10. Here, we assume the intra-band coupling dominant the $\mu_0 H_{c2,c}(T)$ and take the inter-band coupling value $\lambda_{12} = \lambda_{21} = 0.17$ ($\lambda_{12} = \lambda_{21} = 0.13$), and the intra-band coupling value $\lambda_{11} = 0.7$, $\lambda_{22} = 0.3$ ($\lambda_{11} = 0.78$, $\lambda_{22} = 0.3$) for $Ca_{0.83}La_{0.17}FeAs_2$($Ca_{0.8}La_{0.2}Fe_{0.98}Co_{0.02}As_2$). The two-band model can fit the experimental data well as shown in Fig. 4 with $\eta = 7.5$ for $Ca_{0.83}La_{0.17}FeAs_2$ and $\eta = 8$ for $Ca_{0.8}La_{0.2}Fe_{0.98}Co_{0.02}As_2$. The values of η are close to that of SmFeAs(O,F) ($\eta = 9$)[10]. It should be noted that the results here are not sensitive to the choice of the coupling constants as discussed in previous report[9,14,41]. We find that the two-band model can also fit well, even if we change the value of λ properly. Although we can't give the exact coupling values and enable us to analysis the possible pairing scenarios in this novel IBSs, the fitting results by two-gap model can be seen to agree very well with our experimental data.

	T_c (K)	$\mu_0 H^{orb}_{c2,ab}(0)$ (T)	$\mu_0 H^{orb}_{c2,c}(0)$ (T)	$\mu_0 H^{p}_{c2,ab}(0)$ (T)	$\mu_0 H^{*}_{c2,c}(0)$ (T)	ξ_{ab} (0) (nm)	ξ_c (0) (nm)
$Ca_{0.83}La_{0.17}FeAs_2$	40.8	112.5	34.9	84.8	46.8	2.65	1.47
$Ca_{0.8}La_{0.2}Fe_{0.98}Co_{0.02}As_2$	38.8	248	60.9	118.3	88.34	1.93	1.44

Table 1. Superconducting parameters of $Ca_{0.83}La_{0.17}FeAs_2$ and $Ca_{0.8}La_{0.2}Fe_{0.98}Co_{0.02}As_2$ from the analysis of $\mu_0 H_{c2}(T)$. $\mu_0 H^{orb}_{c2}$ (0) denotes the orbital limited $\mu_0 H_{c2}$ at T = 0 K. $\mu_0 H^{p}_{c2,ab}(0)$ denotes the paramagnetically limited $\mu_0 H_{c2}$ at zero-temperature for *H*//ab, which is estimated with the WHH theory including paramagnetism. $\mu_0 H^{*}_{c2,c}(0)$ is the upper critical field for *H*//c, which is determined from fittting the experimental data using the two-band model. ξ_{ab} (0) and ξ_c (0) are the *ab*-plane and *c*-axis zero temperature coherence length calculated using $\mu_0 H^{p}_{c2,ab}(0)$ and $\mu_0 H^{*}_{c2,c}(0)$, respectively.

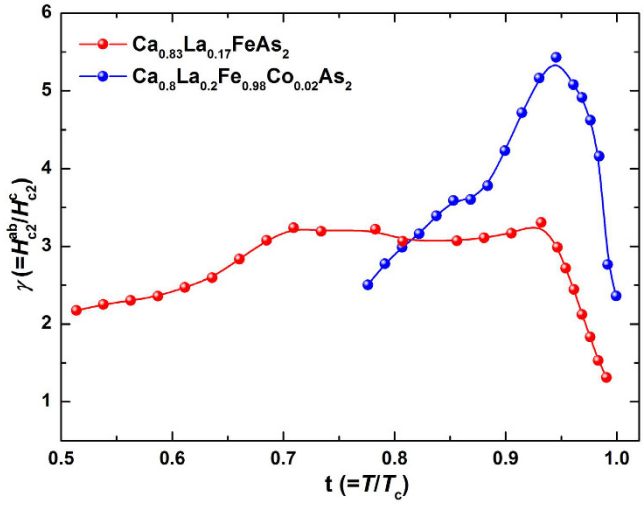

Figure 5. The anisotropic parameter γ versus the reduced temperature T/T_c for $Ca_{0.83}La_{0.17}FeAs_2$ (red circles) and $Ca_{0.8}La_{0.2}Fe_{0.98}Co_{0.02}As_2$ (blue circles) single crystals.

In what follows, we discuss the different temperature dependence of $\mu_0 H_{c2}(T)$ for *H*//*ab* and *H*//*c*, which was generally observed in IBSs[10,13,14,16,17,42,43]. Why the two-band model is essential to explain the behavior of $\mu_0 H_{c2,c}(T)$, but the effect of spin paramagnetic effect is mainly responsible for the behavior of $\mu_0 H_{c2,ab}(T)$, is still unclear now. This calls for further investigations on this interesting question, both experimentally and theoretically. Previous studies have proposed that the cross section of the Fermi surface produces closed current loops that form vortices for *H*//c due to the quasi-two-dimensional Fermi-surface. Thus, the orbital pair-breaking mechanism plays a dominant role in destroying the superconductivity in high magnetic fields, therefore, the two-gap theory, taking into account the orbital pair-breaking effect. In contrast, for *H*//ab, closed loops cannot be easily formed because the cross-sectional area of the Fermi surface is almost fully open with negligible orbital effect, thus, the spin paramagnetic effect is a more dominant factor in $\mu_0 H_{c2,ab}(T)$[10,17]. This scenario seems also to be suitable for this 112-type IBSs since all Fermi-surfaces exhibit two-dimensional character except for the α band[3–5]. Here, we try to give another possible scenario relevant to the spin-locked superconductivity, which has been proposed in quasi-one-dimensional superconductor $K_2Cr_3As_3$[44]. The schematic diagram was shown in SI, Fig. S3. Under this physical scenario, the spins of Cooper pairs are predominantly aligned along the *ab*-plane in IBSs, thus, the behavior of $\mu_0 H_{c2,ab}(T)$ would be pauli-limited. For *H*//*c*, since there is little spin along the c-axis, $\mu_0 H_{c2,c}(T)$ would be hardly effected by the pauli pair-breaking, and mainly restricted by the orbital effect instead. In this case, due to the multiband electronic structure, the enhancement of upper critical field $\mu_0 H_{c2,c}(T)$ should be described by the multiband theory model.

Superconducting parameters of $Ca_{0.83}La_{0.17}FeAs_2$ and $Ca_{0.8}La_{0.2}Fe_{0.98}Co_{0.02}As_2$ obtained from analysis above are summarized in Table 1. Using $\mu_0 H^{p}_{c2,ab}(0)$ and $\mu_0 H^{*}_{c2,c}(0)$, the superconducting coherence length ξ (0) can be estimated using the Ginzburg-Landau formula: $H_{c2,c} = \Phi_0/2\pi\ \xi^2_{ab}(0)$ and $H_{c2,ab} = \Phi_0/2\pi\xi ab(0)\ \xi_c(0)$, where $\Phi_0 = 2.07 \times 10^{-15}$ T m^2 is the flux quantum. We calculated $\xi ab(0) = 2.65$ nm and $\xi_c(0) = 1.47$ nm for $Ca_{0.83}La_{0.17}FeAs_2$, $\xi ab(0) = 1.93$ nm and $\xi_c(0) = 1.44$ nm for $Ca_{0.8}La_{0.2}Fe_{0.98}Co_{0.02}As_2$, respectively. $\xi_c(0)$ of both crystals is larger than the distance *d* (~1.035 nm) between the adjacent FeAs conducting layers, indicating a 3D superconductivity in this novel superconductor, despite the layered nature of their crystal structure.

The temperature dependence of anisotropy of $\mu_0 H_{c2}(T)$ is shown in Fig. 5 as a function of reduced temperature t = T/T_c for $Ca_{0.83}La_{0.17}FeAs_2$ and $Ca_{0.8}La_{0.2}Fe_{0.98}Co_{0.02}As_2$ single crystals. The values of γ reside in the range 1.2~3.2 (2.3 – 5.4) for $Ca_{0.83}La_{0.17}FeAs_2$ ($Ca_{0.8}La_{0.2}Fe_{0.98}Co_{0.02}As_2$) in the temperature region of $T = (0.51 \sim 1)\ T_c$. The anisotropy γ values of both crystals show nonmonotonic temperature-dependent, which first increase and then decrease with decreasing temperature, in consistence with our earlier studies[23]. This strong temperature dependence of γ is similar to that of SmFeAs(O, F), which may originate from the combined effect of two-band

nature and spin paramagnetism[10]. The decreasing γ with decreasing temperature in both crystals results from the enhanced $\mu_0 H_{c2,c}(T)$ and the suppressed $\mu_0 H_{c2,ab}(T)$.

In summary, we have investigated the temperature dependence of upper critical field of $Ca_{0.83}La_{0.17}FeAs_2$ and $Ca_{0.8}La_{0.2}Fe_{0.98}Co_{0.02}As_2$ single crystals under pulsed fields up to 60 T. Analysis based on the WHH model and two-band model indicates that, $\mu_0 H_{c2}(T)$ of this compound bears many similarities to most of IBSs, $\mu_0 H_{c2,ab}(T)$ is clearly limited by the pauli limited effect at low temperatures, and the two-band model is required to describe the enhancement of the upper critical field $\mu_0 H_{c2,c}(T)$. Our work clearly clarifies the behavior of the upper critical field of 112-type iron pnictide superconductors.

Method

Single crystal growth and basic characterizations. Single crystals of $Ca_{0.83}La_{0.17}FeAs_2$ and $Ca_{0.8}La_{0.2}Fe_{0.98}Co_{0.02}As_2$ were grown using the flux method as previous reports[20,22,23]. The single crystal x-ray diffraction (XRD) was performed using a Rigaku diffractometer with Cu $K\alpha$ radiation (see SI, Fig. S1). Elemental analysis was performed by a scanning electron microscope equipped with an energy dispersive x-ray (EDX) spectroscopy probe.

Electrical resistivity measurements. In-plane electrical resistivity was performed by the standard four-probe method in low magnetic field up to 9 T in a Quantum Design Physical Property Measurement System (PPMS-9T) and in pulsed field up to 60 T at Wuhan National High Magnetic Field Center. Golden contacts were made by sputtering in order to provide a low contact resistance (less than 1 Ω.) in the pulsed field measurement.

References

1. Yakita, H. *et al.* A New Layered Iron Arsenide Superconductor: (Ca,Pr)$FeAs_2$. *J. Am. Chem. Soc.* **136,** 846–9 (2014).
2. Katayama, N. *et al.* Superconductivity in $Ca_{1-x}La_xFeAs_2$: A Novel 112-Type Iron Pnictide with Arsenic Zigzag Bonds. *J. Phys. Soc. Jpn.* **82,** 123702 (2013).
3. Wu, X. *et al.* Effect of As-chain layers in CaFeAs2. *Phys. Rev. B* **89,** 205102 (2014).
4. Li, M. Y. *et al.* Significant contribution of As 4 *p* orbitals to the low-lying electronic structure of the 112-type iron-based superconductor $Ca_{0.9}La_{0.1}FeAs_2$. *Phys. Rev. B* **91,** 045112 (2015).
5. Liu, Z. T. *et al.* Observation of the anisotropic Dirac cone in the band dispersion of 112-structured iron-based superconductor $Ca_{0.9}La_{0.1}FeAs_2$. *Appl. Phys. Lett.* **109,** 042602 (2016).
6. Wu, X. *et al.* $CaFeAs_2$: A staggered intercalation of quantum spin Hall and high-temperature superconductivity. *Phys. Rev. B* **91,** 081111(R) (2015).
7. Kamihara, Y., Watanabe, T., Hirano, M. & Hosono, H. Iron-Based Layered Superconductor $La[O_{1-x}F_x]FeAs$ (x = 0.05–0.12) with T_c = 26 K. *J. Am. Chem. Soc.* **130,** 3296–3297 (2008).
8. Jaroszynski, J. *et al.* Upper critical fields and thermally-activated transport of $NdFeAsO_{0.7}F_{0.3}$ single crystal. *Phys. Rev. B* **78,** 174523 (2008).
9. Hunte, F. *et al.* Two-band superconductivity in $LaFeAsO_{0.89}F_{0.11}$ at very high magnetic fields. *Nature* **453,** 903 (2008).
10. Lee, H. S. *et al.* Effects of two gaps and paramagnetic pair breaking on the upper critical field of $SmFeAsO_{0.85}$ and $SmFeAsO_{0.8}F_{0.2}$ single crystals. *Phys. Rev. B* **80,** 144512 (2009).
11. Gurevich, A. Enhancement of the upper critical field by nonmagnetic impurities in dirty two-gap superconductors. *Phys. Rev. B* **67,** 184515 (2003).
12. Fuchs, G. *et al.* High-Field Pauli-Limiting Behavior and Strongly Enhanced Upper Critical Magnetic Fields near the Transition Temperature of an Arsenic-Deficient $LaO_{0.9}F_{0.1}FeAs1$ Superconductor. *Phys. Rev. Lett.* **101,** 237003 (2008).
13. Yuan, H. Q. *et al.* Nearly isotropic superconductivity in $(Ba,K)Fe_2As_2$. *Nature* **457,** 565 (2009).
14. Kano, M. *et al.* Anisotropy of the Upper Critical Field in a Co-Doped $BaFe_2As_2$ Single Crystal. *J. Phys. Soc. Jpn.* **78,** 084719 (2009).
15. Zhang, J. L. *et al.* Upper critical field and its anisotropy in LiFeAs. *Phys. Rev. B* **83,** 174506 (2011).
16. Khim, S. *et al.* Pauli-limiting effects in the upper critical fields of a clean LiFeAs single crystal. *Phys. Rev. B* **84,** 104512 (2011).
17. Ghannadzadeh, S. *et al.* Upper critical field of $NaFe_{1-x}Co_xAs$ superconductors. *Phys. Rev. B* **89,** 054502 (2014).
18. Lei, H., Hu, R., Choi, E. S., Warren, J. B. & Petrovic, C. Pauli-limited upper critical field of $Fe_{1+y}Te_{1-x}Se_x$. *Phys. Rev. B* **81,** 094518 (2010).
19. Lei, H. Iron chalcogenide superconductors at high magnetic fields. *Sci. Technol. Adv. Mater.* **13,** 054305 (2012).
20. Xing, X. *et al.* Anisotropic Ginzburg–Landau scaling of H_{c2} and transport properties of 112-type $Ca_{0.8}La_{0.2}Fe_{0.98}Co_{0.02}As_2$ single crystal. *Supercond. Sci. Technol.* **29,** 055005 (2016).
21. Yakita, H. *et al.* Co and Mn doping effect in polycrystalline (Ca,La) and (Ca,Pr)$FeAs_2$ superconductors. *Supercond. Sci. Technol.* **28,** 065001 (2015).
22. Xing, X. *et al.* Co-co-doping Effect on Superconducting Properties of 112-Type $Ca_{0.8}La_{0.2}FeAs_2$ Single Crystals. *J. Phys. Soc. Jpn.* **84,** 075001 (2015).
23. Zhou, W. *et al.* Anisotropic superconductivity of $Ca_{1-x}La_xFeAs_2$ (x~0.18) single crystal. *Appl. Phys. Express* **7,** 063102 (2014).
24. Kwok, W. K. *et al.* Vortex lattice melting in untwinned and twinned single crystals of $YBa_2Cu_3O_{7-\delta}$. *Phys. Rev. Lett.* **69,** 3370 (1992).
25. Safar, H. *et al.* Experimental evidence for a first-order vortex-lattice-melting transition in untwinned, single crystal $YBa_2Cu_3O_7$. *Phys. Rev. Lett.* **69,** 824 (1992).
26. Sun, Y. *et al.* Critical current density, vortex dynamics, and phase diagram of single-crystal FeSe. *Phys. Rev. B* **92,** 144509 (2016).
27. Sun, Y. *et al.* Large, Homogeneous, and Isotropic Critical Current Density in Oxygen-Annealed $Fe_{1+y}Te_{0.6}Se_{0.4}$ Single Crystal. *Appl. Phys. Express* **6,** 043101 (2013).
28. Vedeneev, S. I., Piot, B. A., Maude, D. K. & Sadakov, A. V. Temperature dependence of the upper critical field of FeSe single crystals. *Phys. Rev. B* **87,** 134512 (2012).
29. Wang, Z. S., Luo, H. Q., Ren, C. & Wen, H. H. Upper critical field, anisotropy, and superconducting properties of $Ba_{1-x}K_xFe_2As_2$ single crystals. *Phys. Rev. B* **78,** 140501(R) (2008).
30. Zhow, W., Xing, X., Wu, W., Zhao, H. & Shi, Z. Second magnetization peak effect, vortex dynamics, and flux pinning in 112-type superconductor $Ca_{0.8}La_{0.2}Fe_{1-x}Co_xAs_2$. *Sci. Rep.* **6,** 22278 (2016).
31. Moll, P. J. W. *et al.* High magnetic-field scales and critical currents in SmFeAs(O, F) crystals. *Nat. Mater.* **9,** 628 (2010).
32. Fuchs, G. *et al.* Orbital and spin effects for the upper critical field in As-deficient disordered Fe pnictide superconductors. *New J. Phys.* **11,** 075007 (2009).
33. Ding, Q. P. *et al.* Magnetic and transport properties of iron-platinum arsenide $Ca_{10}(Pt_{4-\delta}As_8)(Fe_{2-x}Pt_xAs_2)_5$ single crystal. *Phys. Rev. B* **85,** 104512 (2012).
34. Ni, N. *et al.* Anisotropic thermodynamic and transport properties of single-crystalline $Ba_{1-x}K_xFe_2As_2$ (x = 0 and 0.45). *Phys. Rev. B* **78,** 014507 (2008).

35. Sumarlin, I. W. *et al.* Magnetic ordering of Sm in Sm_2CuO_4. *Phys. Rev. Lett.* **68,** 2228 (1992).
36. Maki, K. Effect of Pauli Paramagnetism on Magnetic Properties of High-Field Superconductors*. *Phys. Rev. B* **148,** 362 (1966).
37. Werthamer, N. R., Helfand. E. & Hohenberg, P. C. Temperature and Purity Dependence of the Superconducting Critical Field, H_{c2}. III. Electron Spin and Spin-Orbit Effects. *Phys. Rev.* **147,** 295 (1966).
38. Chandrasekhar, B. S. A note on the maximum critical field of high-field superconductors. *Appl. Phys. Lett.* **1,** 7 (1962).
39. Baily, S. A. *et al.* Pseudoisotropic Upper Critical Field in Cobalt-Doped $SrFe_2As_2$ Epitaxial Films. *Phys. Rev. Lett.* **102,** 117004 (2009).
40. Golubov, A. A. *et al.* Specific heat of MgB_2 in a one- and a two-band model from first-principles calculations. *J. Phys.: Condens. Matter* **14,** 1353 (2002).
41. Li, J. *et al.* High upper critical fields of superconducting $Ca_{10}(Pt_4As_8)(Fe_{1.8}Pt_{0.2}As_2)_5$ whiskers. *Appl. Phys. Lett.* **106,** 262601 (2015).
42. Mun, E. D. *et al.* Anisotropic H_{c2} of $K_{0.8}Fe_{1.76}Se_2$ determined up to 60 T. *Phys. Rev. B* **83,** 100514(R) (2011).
43. Zhang, J. *et al.* Universal behavior of the upper critical field in iron-based superconductors. *Front. Phys.* **6,** 463 (2011).
44. Balakirev, F. F. *et al.* Anisotropy reversal of the upper critical field at low temperatures and spin-locked superconductivity in $K_2Cr_3As_3$. *Phys. Rev. B* **91,** 220505(R) (2015).

Acknowledgements

We gratefully acknowledge the helpful discussions with Dr. Y. Sun. This work was partly supported by the National Natural Science Foundation of China (Grant Nos U1432135, 11674054, 11474080, 11611140101, 11374043 and 11174043), Scientific Research Foundation of Graduate School of Southeast University (Grant No. YBJJ1621), Six-talent Peak of Jiangsu Province (Grants No. 2012-XCL-036), and the open program from Wuhan National High Magnetic Field Center (2015KF15).

Author Contributions

X.Z.X. performed most of the experiments and analyzed the data. The low field resistivity measurement was performed by W.Z. J.H.W. and Z.W.Z. contributed to the pulsed field resistivity measurement at Wuhan National High Magnetic Field Center. Y.F.Z. and N.Z. contributed to the single crystal growth and basic characterization. X.F.X. contributed to the pulsed field data analysis. B.Q. and Z.X.S. designed and directed the research. X.Z.X., B.Q. and Z.X.S. wrote the manuscript. All authors contributed to discussion on the results for the manuscript.

Additional Information

Supplementary information accompanies this paper at http://www.nature.com/srep

Competing Interests: The authors declare no competing financial interests.

How to cite this article: Xing, X. *et al.* Two-band and pauli-limiting effects on the upper critical field of 112-type iron pnictide superconductors. *Sci. Rep.* **7**, 45943; doi: 10.1038/srep45943 (2017).

Publisher's note: Springer Nature remains neutral with regard to jurisdictional claims in published maps and institutional affiliations.